Research Article | Vol. 25, No. 11 | 29 May 2017 | OPTICS EXPRESS 12508
Optics EXPRESS

Third-order gap plasmon based metasurfaces for visible light

RUCHA DESHPANDE,* ANDERS PORS, AND SERGEY I. BOZHEVOLNYI

SDU Nano Optics, University of Southern Denmark, Campusvej 55, DK-5230 Odense M, Denmark
**rad@mci.sdu.dk*

Abstract: Efficient control and manipulation of light using metasurfaces requires high fabrication accuracy that becomes progressively demanding when decreasing the operation wavelength. Considering gap surface plasmon (GSP) based metasurfaces, we demonstrate that the metasurfaces, which utilize the third-order GSP resonance and thereby involve relatively large nanobricks, can successfully be used for efficient polarization-controlled steering of visible light. The reflection amplitude and phase maps for a 450 nm period array of 50 nm thick nanobricks placed atop a 40 nm thick silica layer supported by an optically thick gold film are calculated for the operation wavelength of 633 nm. Exploiting the occurrence of the third-order GSP resonance for nanobricks having their lengths close to 300 nm, we design the phase-gradient metasurface, representing an array of (450 x 2250 nm^2) supercells made of 5 nanobricks with different dimensions, to operate as a polarization beam splitter for linearly polarized light. The fabricated polarization beam splitter is characterized using a supercontinuum light source at the normal light incidence and found to exhibit a polarization contrast ratio of up to 40 dB near the design wavelength of 633 nm while showing better than 20 dB contrast in the range of 550 – 650 nm for both polarizations. The diffraction efficiency experimentally measured at normal incidence exceeds 10% (20% in simulations) at the design wavelength of 633 nm, with the performance for the TE polarization (electric field perpendicular to the plane of diffraction) being significantly better (experimentally > 20% and theoretically > 40%) than for the TM polarization. This difference becomes even more pronounced for the light incidence deviating from normal. Finally, we discuss possible improvements of the performance of polarization beam splitters based on third-order GSP resonance as well as other potential applications of the suggested approach.

OCIS codes: (250.5403) Plasmonics; (310.6628) Subwavelength structures, nanostructures; (130.5440) Polarization-selective devices; (160.3918) Metamaterials.

References and links

1. S. B. Glybovski, S. A. Tretyakov, P. A. Belov, Y. S. Kivshar, and C. R. Simovski, "Metasurfaces: from microwave to visible," Phys. Rep. **634**, 1–72 (2016).
2. H.-T. Chen, A. J. Taylor, and N. Yu, "A review of metasurfaces: physics and applications," Rep. Prog. Phys. **79**(7), 076401 (2016).
3. L. Lin, X. M. Goh, L. P. McGuinness, and A. Roberts, "Plasmonic lenses formed by two-dimensional nanometric cross-shaped aperture arrays for Fresnel-region focusing," Nano Lett. **10**(5), 1936–1940 (2010).
4. A. Pors, M. G. Nielsen, R. L. Eriksen, and S. I. Bozhevolnyi, "Broadband focusing flat mirrors based on plasmonic gradient metasurfaces," Nano Lett. **13**(2), 829–834 (2013).
5. A. Pors, M. G. Nielsen, G. D. Valle, M. Willatzen, O. Albrektsen, and S. I. Bozhevolnyi, "Plasmonic metamaterial wave retarders in reflection by orthogonally oriented detuned electrical dipoles," Opt. Lett. **36**(9), 1626–1628 (2011).
6. Y. Zhao and A. Alù, "Manipulating light polarization with ultrathin plasmonic metasurfaces," Phys. Rev. B **84**(20), 205428 (2011).
7. A. Roberts and L. Lin, "Plasmonic quarter-wave plate," Opt. Lett. **37**(11), 1820–1822 (2012).
8. P.-C. Li, Y. Zhao, A. Alù, and E. T. Yu, "Experimental realization and modeling of a subwavelength frequency selective plasmonic metasurface," Appl. Phys. Lett. **99**(22), 221106 (2011).
9. P.-C. Li and E. T. Yu, "Wide-angle wavelength-selective multilayer optical metasurfaces robust to interlayer misalignment," J. Opt. Soc. Am. B **30**(1), 27–32 (2013).
10. A. Pors, F. Ding, Y. Chen, I. P. Radko, and S. I. Bozhevolnyi, "Random-phase metasurfaces at optical wavelengths," Sci. Rep. **6**(1), 28448 (2016).

#287368 https://doi.org/10.1364/OE.25.012508
Journal © 2017 Received 28 Feb 2017; revised 1 May 2017; accepted 2 May 2017; published 19 May 2017

Optics EXPRESS

11. J. Zheng, Z. C. Ye, N. L. Sun, R. Zhang, Z. M. Sheng, H. P. Shieh, and J. Zhang, "Highly anisotropic metasurface: a polarized beam splitter and hologram," Sci. Rep. **4**(1), 6491 (2015).
12. A. Pors, M. G. Nielsen, and S. I. Bozhevolnyi, "Plasmonic metagratings for simultaneous determination of stokes parameters," Optica **2**(8), 716–723 (2015).
13. A. Pors and S. I. Bozhevolnyi, "Plasmonic metasurfaces for efficient phase control in reflection," Opt. Express **21**(22), 27438–27451 (2013).
14. N. M. Estakhri and A. Alù, "Recent progress in gradient metasurfaces," J. Opt. Soc. Am. B **33**(2), A21–A30 (2016).
15. N. Yu, P. Genevet, M. A. Kats, F. Aieta, J. P. Tetienne, F. Capasso, and Z. Gaburro, "Light propagation with phase discontinuities: generalized laws of reflection and refraction," Science **334**(6054), 333–337 (2011).
16. X. Ni, N. K. Emani, A. V. Kildishev, A. Boltasseva, and V. M. Shalaev, "Broadband light bending with plasmonic nanoantennas," Science **335**(6067), 427 (2012).
17. N. Yu, F. Aieta, P. Genevet, M. A. Kats, Z. Gaburro, and F. Capasso, "A broadband, background-free quarter-wave plate based on plasmonic metasurfaces," Nano Lett. **12**(12), 6328–6333 (2012).
18. F. Aieta, P. Genevet, M. A. Kats, N. Yu, R. Blanchard, Z. Gaburro, and F. Capasso, "Aberration-free ultrathin flat lenses and axicons at telecom wavelengths based on plasmonic metasurfaces," Nano Lett. **12**(9), 4932–4936 (2012).
19. M. V. Berry, "The adiabatic phase and Pancharatnam's phase for polarized light," J. Mod. Opt. **34**(11), 1401–1407 (1987).
20. Z. Bomzon, G. Biener, V. Kleiner, and E. Hasman, "Space-variant Pancharatnam-Berry phase optical elements with computer-generated subwavelength gratings," Opt. Lett. **27**(13), 1141–1143 (2002).
21. Y. Wang, M. Pu, Z. Zhang, X. Li, X. Ma, Z. Zhao, and X. Luo, "Quasi-continuous metasurface for ultra-broadband and polarization-controlled electromagnetic beam deflection," Sci. Rep. **5**(1), 17733 (2016).
22. C. Pfeiffer and A. Grbic, "Metamaterial Huygens' surfaces: tailoring wave fronts with reflectionless sheets," Phys. Rev. Lett. **110**(19), 197401 (2013).
23. C. Pfeiffer, N. K. Emani, A. M. Shaltout, A. Boltasseva, V. M. Shalaev, and A. Grbic, "Efficient light bending with isotropic metamaterial Huygens' surfaces," Nano Lett. **14**(5), 2491–2497 (2014).
24. F. Monticone, N. M. Estakhri, and A. Alù, "Full control of nanoscale optical transmission with a composite metascreen," Phys. Rev. Lett. **110**(20), 203903 (2013).
25. X. Ding, F. Monticone, K. Zhang, L. Zhang, D. Gao, S. N. Burokur, A. de Lustrac, Q. Wu, C. W. Qiu, and A. Alù, "Ultrathin Pancharatnam-Berry metasurface with maximal cross-polarization efficiency," Adv. Mater. **27**(7), 1195–1200 (2015).
26. T. Søndergaard, J. Jung, S. I. Bozhevolnyi, and G. Della Valle, "Theoretical analysis of gold nano-strip gap plasmon resonators," New J. Phys. **10**(10), 105008 (2008).
27. T. Søndergaard and S. I. Bozhevolnyi, "Strip and gap plasmon polariton optical resonators," Phys. Status Solidi, B Basic Res. **245**(1), 9–19 (2008).
28. M. G. Nielsen, D. K. Gramotnev, A. Pors, O. Albrektsen, and S. I. Bozhevolnyi, "Continuous layer gap plasmon resonators," Opt. Express **19**(20), 19310–19322 (2011).
29. A. Pors, O. Albrektsen, I. P. Radko, and S. I. Bozhevolnyi, "Gap plasmon-based metasurfaces for total control of reflected light," Sci. Rep. **3**(1), 2155 (2013).
30. S. I. Bozhevolnyi and T. Søndergaard, "General properties of slow-plasmon resonant nanostructures: nano-antennas and resonators," Opt. Express **15**(17), 10869–10877 (2007).
31. P. B. Johnson and R. W. Christy, "Optical constants of the noble metals," Phys. Rev. B **6**(12), 4370–4379 (1972).
32. A. Pors and S. I. Bozhevolnyi, "Gap plasmon-based phase-amplitude metasurfaces: material constraints," Opt. Mater. Express **5**(11), 2448–2458 (2015).
33. Q. T. Li, F. Dong, B. Wang, F. Gan, J. Chen, Z. Song, L. Xu, W. Chu, Y. F. Xiao, Q. Gong, and Y. Li, "Polarization-independent and high-efficiency dielectric metasurfaces for visible light," Opt. Express **24**(15), 16309–16319 (2016).
34. P. West, S. Ishii, G. Naik, N. Emani, V. Shalaev, and A. Boltasseva, "Searching for better plasmonic materials," Laser Photonics Rev. **4**(6), 795–808 (2010).
35. G. V. Naik, V. M. Shalaev, and A. Boltasseva, "Alternative plasmonic materials: Beyond gold and silver," Adv. Mater. **25**(24), 3264–3294 (2013).
36. S. Astilean, P. Lalanne, P. Chavel, E. Cambril, and H. Launois, "High-efficiency subwavelength diffractive element patterned in a high-refractive-index material for 633 nm," Opt. Lett. **23**(7), 552–554 (1998).
37. D. Lin, P. Fan, E. Hasman, and M. L. Brongersma, "Dielectric gradient metasurface optical elements," Science **345**(6194), 298–302 (2014).
38. R. C. Devlin, M. Khorasaninejad, W. T. Chen, J. Oh, and F. Capasso, "Broadband high-efficiency dielectric metasurfaces for the visible spectrum," Proc. Natl. Acad. Sci. U.S.A. **113**(38), 10473–10478 (2016).
39. M. Khorasaninejad, A. Y. Zhu, C. Roques-Carmes, W. T. Chen, J. Oh, I. Mishra, R. C. Devlin, and F. Capasso, "Polarization-insensitive metalenses at visible wavelengths," Nano Lett. **16**(11), 7229–7234 (2016).
40. Z. Wang, S. He, Q. Liu, and W. Wang, "Visible light metasurfaces based on gallium nitride high contrast gratings," Opt. Commun. **367**, 144–148 (2016).
41. T. Søndergaard and S. Bozhevolnyi, "Slow-plasmon resonant nanostructures: Scattering and field enhancements," Phys. Rev. B **75**(7), 073402 (2007).

Optics EXPRESS

42. R. Gordon, "Light in a subwavelength slit in a metal: Propagation and reflection," Phys. Rev. B **73**(15), 153405 (2006).
43. S. Larouche and D. R. Smith, "Reconciliation of generalized refraction with diffraction theory," Opt. Lett. **37**(12), 2391–2393 (2012).
44. F. Qin, L. Ding, L. Zhang, F. Monticone, C. C. Chum, J. Deng, S. Mei, Y. Li, J. Teng, M. Hong, S. Zhang, A. Alù, and C.-W. Qiu, "Hybrid bilayer plasmonic metasurface efficiently manipulates visible light," Sci. Adv. **2**(1), e1501168 (2016).
45. Y. Dai, W. Ren, H. Cai, H. Ding, N. Pan, and X. Wang, "Realizing full visible spectrum metamaterial half-wave plates with patterned metal nanoarray/insulator/metal film structure," Opt. Express **22**(7), 7465–7472 (2014).
46. Z. Li, E. Palacios, S. Butun, and K. Aydin, "Visible-frequency metasurfaces for broadband anomalous reflection and high-efficiency spectrum splitting," Nano Lett. **15**(3), 1615–1621 (2015).

1. Introduction

The desire to control optical properties of light at miniature scale has given rise to the intensive research within nanophotonics, which is at the heart of modern optical technologies. One of the most important developments that opened new routes for optical design, photonic materials, and unique functionalities is associated with metasurfaces, which are planar (two-dimensional) metamaterials composed of optically thin and densely packed planar arrays of subwavelength elements [1,2]. The field of metasurfaces shows growing interest due to their compatibility with commercial nanofabrication techniques and relatively low losses along with easy to design techniques available to control properties of light. One can distinguish dielectric and plasmonic metasurfaces, of which the latter consists of metal nanostructures that by virtue of supporting deeply subwavelength resonant modes allow one to realize ultra-thin metasurfaces with fine phase/amplitude discretization in the metasurface plane and thereby very large numerical apertures in the resulting optical elements [2]. Plasmonic metasurfaces operating at wavelengths ranging from visible to microwave [2] and exhibiting diverse functionalities, such as lenses [3], focusing mirrors [4], waveplates [5–7], wavelength selective surfaces [8,9], random phase reflectors [10], polarization beam splitters and holograms [11,12] have been demonstrated.

It is observed for plasmonic metasurfaces that, most often, the achievable phase variation in the reflected/transmitted light is restricted to π, since resonant elements constituting the metasurface possess a Lorentzian-like polarizability [5,6]. The complete 2π phase control desirable in gradient metasurface-based applications can be achieved by three common ways [13,14]. In the first way, phase up to 2π and amplitude of light can be manipulated by influencing the polarization state of incident light using nanoantennas as optical resonators to produce cross-polarization and anisotropic scattering property of Pancharatnam-Berry phase (PB) elements [15,16]. The fabrication of nanoantennas and meta-scatteres that have similar geometry but spatially varying optic axis using the design of proper phase shift based on "Generalized laws of reflection and refraction" [15] has led to many applications of phase-gradient based metasurfaces including beam deflection, polarization conversion and aberration-free lenses [15–20]. The P-B phase metasurfaces have demonstrated broadband applications due to the advantage that design wavelength depends only on the size of meta-elements [21]. The second way to achieve 2π phase control is to design multiple layers based on tuning of electric and magnetic polarizabilities to have the same impedance as surrounding media called Huygens metasurface [22]. It is analogous to the approach of "Frequency Selective Surfaces" (FSS) for radio frequencies, and by scaling it to lower frequencies it is recently demonstrated in the optical regime to reduce the reflection losses in transmitting metasurfaces [23]. Nevertheless, the planar transmitting metasurfaces have a theoretical upper limit of 25% efficiency despite ignoring material and fabrication losses [24,25]. The third possible way to obtain 2π phase control with high efficiency consists of metal substrate backed metasurfaces that operate in reflection [13]. These metasurfaces are based on the metal-insulator-metal (MIM) configurations supporting Fabry-Perot-like resonances due to the reflection of gap surface plasmons (GSPs) by MIM terminations because of strong GSP index mismatch with the surrounding [26–28]. Depending on the geometrical parameters of

Optics EXPRESS

these MIM configurations (termed GSP resonators), consisting of metal nanobricks atop thin spacer and optically thick metal layers, one can achieve high efficiencies (close to 100%) in near-IR wavelength region [29].

A remarkable fact that makes plasmonic metasurfaces attractive for future technologies is that they can be designed to operate at any wavelength by properly scaling geometrical dimensions of individual elements in the surface plane. For instance, in plasmonic resonators using IMI or MIM configurations, the resonator width scales linearly with the resonance wavelength [27,30]. This trend leads however to fabrication problems as we reach the visible wavelength regime, where the feature sizes become progressively small and challenging to be fabricated using available nanofabrication techniques. There is also another challenge to face when designing metasurfaces for operation in the visible region (500 - 700 nm): high operation efficiency requires relatively low ohmic losses in the metal used to fabricate metasurface in [31–33] and references within. To address the latter problem, there is ongoing research to find alternative materials, which have low losses and good compatibility with fabrication techniques [34,35]. In addition, the use of dielectric materials have shown an increase in efficiency of metasurfaces especially transmissive metasurfaces [36–38]. Notably, titanium dioxide (TiO_2) on fused silica substrate, gallium nitride (GaN) for application of lenses [39,40] and silicon dioxide (SiO_2) based metasurface holograms [39] demonstrate efficiency reaching 90% for visible wavelengths. However, the feature sizes of fabricated metasurfaces demonstrating highest efficiency still demand accuracy of ~5 - 10 nm [37–39].

Here, we propose a new approach for increasing metasurface element dimensions and thereby relaxing fabrication constraints by using higher order, e.g., third-order GSP resonances to fabricate gradient metasurfaces operating in the visible spectral range. We first perform numerical studies of fundamental and third-order GSP resonances to explore both the possibility and need to use higher order resonances. Then, after designing a unit cell to diffract the orthogonal linear polarizations into different diffraction orders, we fabricate and characterize the designed metasurface with respect to the polarization contrast and overall diffraction efficiency at normal as well as varying incident angles. Finally, we discuss possible improvements of the performance of polarization beam splitters based on third-order GSP resonances as well as other potential applications of the suggested approach.

2. Third-order gap surface plasmon resonance

The interaction of light with metasurface based on fundamental GSP resonances arising in metal backed 2D planar metal nanobrick separated by thin spacer layer (MIM) configuration has been extensively studied in the past [26–28]. The configuration as represented in Fig. 1(a) shows a metal backed planar metasurface that can control reflected light up to 2π phase span most efficiently [29]. Its applicability at visible wavelengths is practically limited and can be overcome using third-order GSP resonances, which to our best knowledge have not been studied in detail before.

We begin by describing the nature of GSP resonances. Metal-dielectric interfaces support electromagnetic waves in the form of gap surface plasmons, which are reflected due to strong effective index mismatch between GSP and the surroundings, and travel back and forth along structure terminations of metasurface producing standing wave like resonances called GSP resonances. The GSP resonances can be described by simple Fabry-Pérot resonator formula as given below [41,42]:

$$wk_0 n_{gsp} + \varphi = p\pi \tag{1}$$

where, w describes the width of the nanobrick, k_0 is the vacuum wave number, n_{gsp} is the real part of the effective refractive index of the GSP, which depends on the material parameters as well as t and t_s, p is an integer defining the order of the GSP mode, φ is an additional phase shift that accounts for the fact that GSPs are not immediately reflected from the physical boundaries of the MIM configuration as part of the field extends outside the structure.

Optics EXPRESS

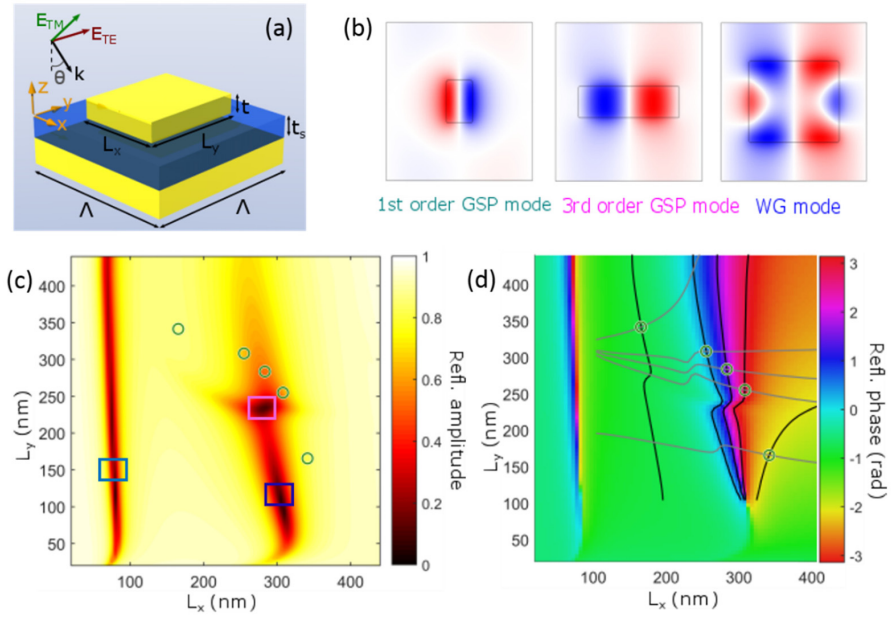

Fig. 1. Reflection amplitude and phase map of third-order GSP-based metasurface. (a) Sketch of a basic unit cell consisting of metal nanobrick (composed of gold, thickness t) having nanobrick width *w* in two dimensions L_x and L_y in x-y plane on top of a glass spacer (SiO_2, refractive index 1.45, thickness t_s) and metal substrate (optically thick). (b) The magnitude of z-component of the electric field in the center of the spacer in the xy-plane showing mode profile of fundamental mode, third-order mode and whispering gallery (WG) mode indicated by square markings in Fig. 1. (c). (c, d) Calculated reflection and phase coefficients as a function of nanobrick widths for Λ = 450 nm, t_s = 40 nm, t = 50 nm, wavelength (λ) = 633 nm when TM polarized light is normally incident. The circles indicate the geometrical parameters (L_x, L_y) for which phase values are same for both TM and TE polarizations covering phase in equal steps of 70° between adjacent elements and high reflection amplitude most suitable for the design of metasurface.

In order to study the optical properties of both (p = 1) fundamental and (p = 3) third-order resonance for visible wavelength of 633 nm, we consider the unit cell composed of gold-SiO_2-gold having optically thick bottom gold layer, thin spacer layer of (t_s = 40 nm) and variable nanobrick width dimensions (L_x, L_y) on top of metasurface illuminated by normal incident light. The nanobrick dimensions (L_x, L_y) are the only variable parameters while other geometrical parameters are kept constant. The permittivity of gold is obtained by interpolation of experimental data by Johnson and Christy [31] and the refractive index of glass is taken to be 1.45. Using this data, we perform simulations using commercially available software COMSOL Multiphysics to obtain complex reflection and phase coefficients as shown in Fig. 1 (c, d). The characteristic features of GSP resonance are quickly realized by local enhancement of electric field inside the spacer layer along the nanobricks depending on dimensions (L_x, L_y). These are observed in the form of mode profile for both fundamental and third-order resonances showing one and three nodes, respectively as shown in Fig. 1(b). In addition, strong dip in the amplitude of complex reflection coefficient is observed at both resonances accompanied by simultaneous 2π phase change contributed by Lorentz-like π phase response of oscillator and its efficient back reflection from bottom gold layer [Fig. 1(c, d)]. It is evident that the properties of GSP resonances at visible wavelengths are responsible for the very narrow fundamental resonance of feature sizes within 60 - 100 nm, demanding very high fabrication accuracy of < 5 nm, which is difficult to fabricate using current nanofabrication techniques. On the contrary, third-order resonance covers a broad range of feature sizes from 200 - 400 nm and is practically realizable depending on

Optics EXPRESS

fabrication constraints as can be observed from Fig. 1(c, d). The numerical simulations performed for orthogonal polarizations (TM and TE, along x and y-axis of nanobrick) demonstrate that visible light can be controlled up to 2π phase space within practically realizable nanobrick dimensions (L_x, L_y) fulfilling the requirement for optical devices having desirable functionalities like polarization splitting [11], waveplates [5–7], lenses [3] and mirrors [4]. The nature of third-order resonance as seen in Fig. 1(b) shows a new feature close to it and detailed calculations indicate that it is a mixed mode occurring due to rectangular edges of nanobricks forming a whispering gallery (WG mode). The detailed optical properties of WG mode are not a part of this discussion, as it does not affect the functionality of 2π phase space shown by third-order resonance.

3. Design and fabrication of metasurface

In designing the metasurface at a visible wavelength of 633 nm, we have carefully chosen the subwavelength period of the supercell to be Λ = 450 nm. It fulfills the local periodicity assumption, ensures weak coupling between individual nanobrick elements and allows GSP resonant characteristics for each of them to be strongly pronounced in the supercell. Low diffraction orders ($\Theta_{\pm 1} = 16.3^o$) making the metasurface suitable for optical characterization are also facilitated by the period of metasurface. In the design of metasurface as a polarization splitter, the phase gradient up to 2π along the supercell plays a key role. This requirement is fulfilled by the metal backed MIM configuration with good efficiency. The simulation of third-order GSP resonances based on the MIM configuration when TM polarized light is incident are shown in Fig. 1(c, d). Similar simulation for TE polarized incident light is also performed. We then used a search algorithm to locate the phase values for which both orthogonal polarizations have same geometrical parameters (L_x, L_y). These are represented as intersections of lines of a constant phase gradient shown in Fig. 1(d). It can be seen that the phase values discretize the supercell into five elements having phase gradient in the interval of 70^o with the unique feature that the direction of the gradient is opposite for the two orthogonal polarizations. This gradient in phase can be viewed as phase blazed grating which reflects the orthogonal polarizations of linearly polarized light into two opposite directions with respect to normal from the metasurface fulfilling the functionality of metasurface as polarization splitter [11,12]. The individual elements of the phase gradient arranged periodically (Λ = 450 nm) composing the supercell of the metasurface is shown in Fig. 2(a). The simulation of reflected electric field showing x-axis oriented TM polarized light and y-axis oriented along TE polarized light very close to the metasurface can be seen in Fig. 2(b,c). Since the nanobricks near the GSP resonance have a more pronounced dip in amplitude, there are more pronounced absorption losses making the reflection amplitude position-dependent within the supercell comprising the metasurface. Ideally, the amplitude for all these elements must be constant but the simplicity of the design of our metasurface allows us to have practical control of either the phase or the amplitude.

Optics EXPRESS

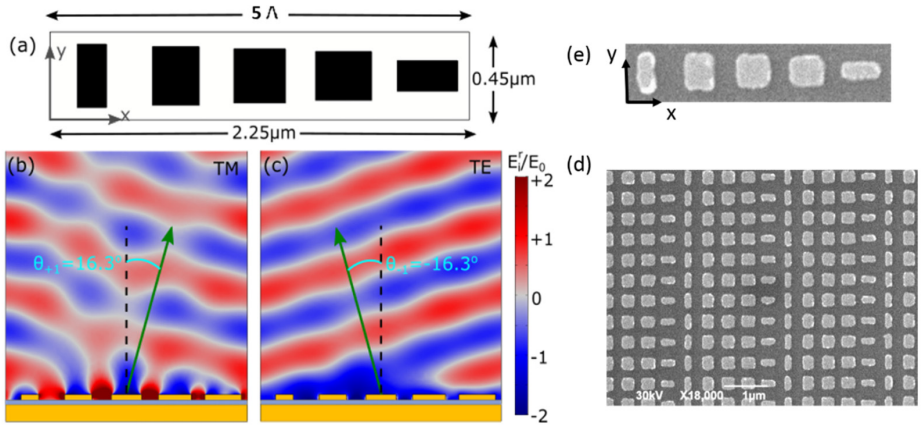

Fig. 2. Design and fabrication of metasurface. (a) The geometry of supercell designed at 633 nm wavelength to split linearly polarized light. (b, c) Simulations showing the x-component E_x^r (TM) and y-component E_y^r (TE) of the electric field, respectively just above metasurface at the design wavelength of 633 nm (the amplitude of incident E-field is 1 V/m). The components are reflected into two diffraction orders (m = + 1, −1, respectively). (d) Image of a fabricated array of unit cells of metasurface using Scanning Electron Microscopy (SEM). (e) Inset showing single fabricated unit cell.

We used Electron Beam Lithography (EBL) nanofabrication technique to fabricate the metasurface, which comprises an array of supercells. In this technique, thin layers of metals viz. gold, titanium and dielectric spacer silicon dioxide (SiO_2) are deposited using e-beam evaporation and RF sputtering, respectively on Si-wafer substrate. Adhesion is facilitated by deposition of 3 nm titanium within the layers. A positive resist 950 kDa PMMA commercially purchased is deposited onto the sample using a spin coater to obtain a thickness of 100 nm. The resist is then exposed to the pattern designed for the metasurface using scanning electron microscope (SEM, model: JEOL JSM-6490LV) with acceleration voltage 30 KV, working distance 9 mm, area dose of 200 μC/cm^2, write field 100 x 100 μm^2 and step size of 2 nm. After exposure, the resist is developed for 30 s in a 3:1 mixture of isopropanol (IPA): methyl isobutyl ketone (MIBK). Nanobricks of 50 nm height are fabricated by deposition of gold using e-beam evaporation and subsequent 10 hours incubation in acetone for lift-off of unexposed resist. The fabricated metasurface ready for optical characterization is imaged using scanning electron microscopy (SEM) as shown in Fig. 2(d, e). From the figure, it can be seen that the metasurfaces are very well fabricated with rectangular shapes of the nanobricks well formed. The roughness and rounding at the edges of nanobricks are the only possible ways that can lead to losses due to fabrication and previous literature shows that 100% efficiency was obtained in spite of that [29]. Good quality fabrication can be achieved by using advanced EBL systems and perhaps combining them with annealing. It is most remarkable that we have achieved such good quality fabrication for visible wavelength region by tackling the problem of scaling down of feature sizes using third-order GSP resonance.

4. Results and discussion

The experimental verification of the metasurface is performed using the optical set-up as shown below in Fig. 3. The metasurface (x-y plane) and the detector (x-z plane) are placed at two different concentric rotating arms which allow effective optical characterization of the metasurface for normal as well as varying incident angle. White light from SuperK laser source is incident onto the sample using the focusing lens (f = 10 cm) slightly before focus ensuring that the spot is within the metasurface. The control of incident polarization is achieved using an assembly of two Glan-Thomson polarizers and use of quarter wave plate located between them to control power for each of the polarization. As the laws of

Optics EXPRESS

generalized reflection and refraction together with diffraction theory allows one to consider the metasurface grating to be a phase blazed grating [43], the different diffraction orders including the zero order are reflected into different directions with respect to normal from metasurface. The metasurface is designed to allow TE and TM orthogonal polarizations to be reflected along m = ± 1 diffraction orders and by using linear polarizer we also verify their state of polarization after reflection from metasurface. The other diffraction orders including m = 0 and higher diffraction orders m = ± 2, ± 3… consist of mixed state of polarization and are part of losses. Optical images for the m = ± 1 diffraction order and the zero order are shown in Fig. 3(a, b) when the angle of incidence is approximately 10°. For normal incidence and smaller angles of incidence, we used a non-polarizing polarization beam splitter to collect the back reflected or blocked diffraction orders. In Fig. 3(a), we show the image of contrast between diffraction order with the presence of strong polarization and weaker spot containing mixed polarization state having reversible positions after splitting for TM and its counterpart TE polarization, which is clearly seen for incident light of design wavelength 633 nm. The zero diffraction order is blocked in the image for clear visualization of the contrast. In Fig. 3(b), splitting of individual polarizations into main diffraction orders m = + 1, 0, −1 for an incident white light source having individual polarizations are shown. During the experiments, we ensured that individual incident polarizations have equal power.

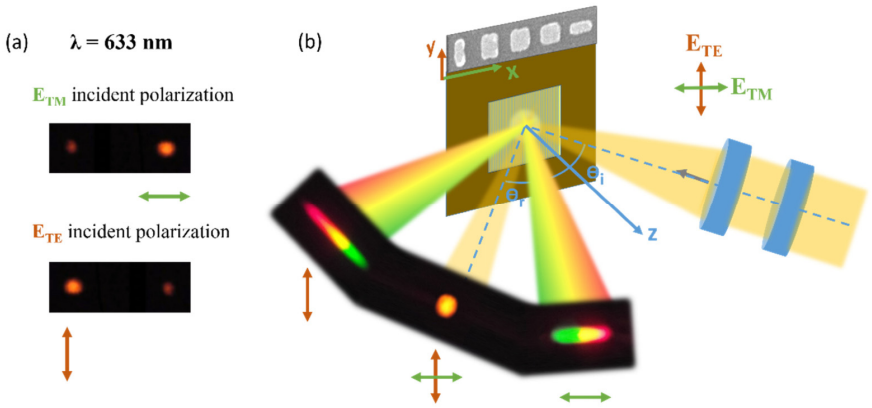

Fig. 3. Experimental setup for optical characterization of metasurface as polarization splitter for linearly polarized light (E_{TE} and E_{TM} being the two orthogonal components). (a) Optical image of light reflected from metasurface when individual polarization is incident (source is a laser of 633 nm wavelength). The zero order is blocked in the image to allow for clear visualization of contrast. (b) Reflected light from metasurface imaged when the light of both polarizations are incident. The setup comprises of white light from SuperK laser passing through an optical system consisting of polarizers and a focusing lens. The light is incident at 0° as well as different angles with respect to normal (z-axis) from metasurface plane (x and y-axes).

The results for optical characterization of metasurface for polarization splitting functionality are shown in Fig. 4 and 5. The amount of light reflected into a diffraction order given by reflectance for normal incident white light is shown in Fig. 4(a, b). It is the ratio of the intensity of reflected light of individual diffraction order to the intensity of light reflected from plain gold surface acting as a reference reflector. It gives an account of diffraction efficiency of the metasurface. It can be seen from the Fig. 4(a, b) that the performance for TE polarization shows 40% efficiency based on simulations and > 20% experimentally which is significantly better compared with TM polarization for normal incident angle and at the design wavelength of 633 nm. This value of efficiency is also in good agreement with the efficiency of other metasurfaces fabricated for visible wavelength region using gold as plasmonic material [44]. Significant improvement in efficiency has been reported by use of silver as plasmonic material [45,46]. It can be seen that the use of third-order GSP resonances

Optics EXPRESS

is most practicable for designing metasurfaces as it relaxes fabrication constraints by improving the feature sizes of meta-elements and has reasonably good efficiency. Despite the slight variation in diffraction efficiency, the functionality of metasurface as polarization splitter shows good efficiency with the desired polarization > 3 orders of magnitude higher compared to unwanted polarization. This can be seen from Fig. 4(c, d) which displays the ratio of the intensity of desired polarization to unwanted polarization, which in the experiments correspond to ± 1 diffraction orders. The effectiveness of the polarization splitter is relatively constant for the broad wavelength range from 580 nm to 680 nm (100 nm) for TE polarization and up to 665 nm for TM polarization covering almost half the visible spectrum from green to red light. The decrease in performance for wavelengths lower than 633 nm design wavelength is prominently due to a decrease in diffraction efficiency. For higher wavelengths, the performance is affected due to a decrease in efficiency as well as an increase of intensity from higher diffraction orders comprising of unwanted polarization state.

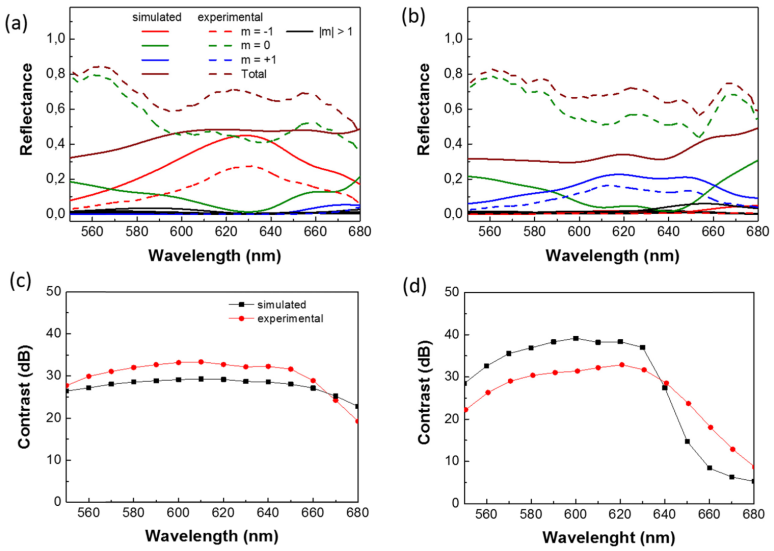

Fig. 4. Optical characterization of metasurface. (a, b) The amount of light reflected from the metasurface for different visible wavelengths at normal incident angle. (c, d) The amount of desired polarized light compared to unwanted polarized light reflected from metasurface when individual polarizations are incident on the metasurface at normal incident angles for different visible wavelengths. ((a, c) correspond to TE incident polarized light and (b, d) TM polarized light).

It is seen that, except for the zero order, all the diffraction orders follow a similar trend as the results obtained from simulation of metasurface. This discrepancy between simulated and experimental values can be accounted for the fact that optical properties of evaporated gold for visible wavelength are not known very well and it could be an effect of the use of higher order GSP resonances. In our study, we explore the angle dependent sensitivity of our metasurface, which is a useful property for all applications. We found that for different angles of incidence, the performance for TM polarized light decreases rapidly as can be seen from the increase in higher diffraction orders from Fig. 5(b). On the contrary, the performance for TE polarized light remains constant up to a 30^{o} angle of incidence as shown in Fig. 5(b). The weak performance of reflected TM polarized light can be attributed to the fact that its electric field lies in the x-z plane, which coincides with the direction of the phase gradient affecting the local periodicity assumption. This angle dependent sensitivity of polarization splitter can be very useful in many optical devices like filters and selective absorption in plasmonic solar cells. So far, very few studies have been performed to determine if metasurfaces can be sensitive to angle of incidence.

Optics EXPRESS

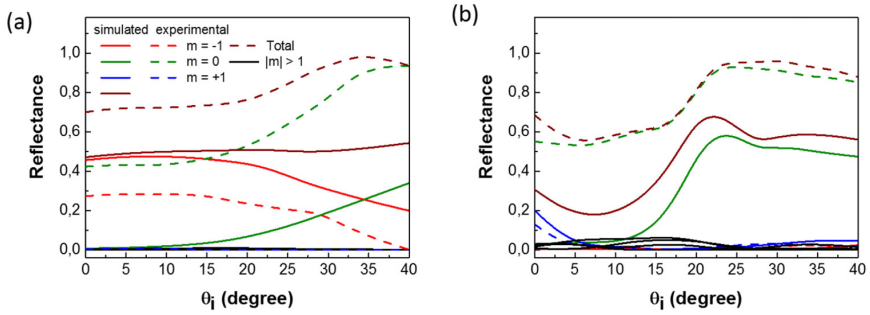

Fig. 5. Optical characterization of metasurface for varying angle of incidence at 633 nm incident wavelength. (a) The amount of light reflected into different diffraction orders as a function of the angle of incidence for TE incident polarization and (b) TM incident polarization.

5. Conclusion

In summary, we have demonstrated that plasmonic phase-gradient metasurfaces, which utilize the third-order GSP resonance and thereby involve relatively large nanobricks (so that the fabrication constraints are relaxed), can successfully be used for efficient polarization-controlled steering of visible light. The fabricated polarization beam splitter is characterized using a supercontinuum light source at the normal light incidence and found to exhibit a polarization contrast ratio of up to 40 dB near the design wavelength of 633 nm while showing better than 20 dB contrast in the range of 550 – 650 nm for both polarizations. The diffraction efficiency experimentally measured at normal incidence exceeds 10% (20% in simulations) at the design wavelength of 633 nm, with the performance for the TE polarization being significantly better (experimentally > 20% and theoretically > 40%) than for the TM polarization. The deterioration of the performance for the TM polarization is expected due to a simplified design procedure in which, the phase (specular) of reflected light under the normal incidence is determined (Fig. 1.) so that only the electric field components parallel to the surface plane are considered (whereas the diffraction of the TM polarization involves the field components perpendicular to the surface plane). By implementing complicated design procedures and also use of silver [45,46] or other suitable plasmonic materials, significant improvement in the efficiency of the metasurface can be achieved. Our metasurface can have many interesting applications including measurements of the amount of linearly polarized light along with the polarization-controlled splitting of linearly polarized light. The angular dependence of the diffraction efficiency can be used for selective light absorption in devices like solar cells and has scope to improve upon previous applications. The concept of using higher order resonances for the design of metasurfaces is new, and our study shows that one can advantageously make use of it for metasurfaces operating in the visible spectral range for relaxing the fabrication constraints.

Funding

H2020 European Research Council (ERC) (Grant No. 341054 (PLAQNAP)); University of Southern Denmark (SDU2020).

Acknowledgments

The authors would like to thank S. K. H. Andersen for the help with fabrication techniques and V. A. Zenin for the help with the optical set-up alignment.